tadata, citation and similar papers at core.ac.uk

ELSEVIER

Materials Science and Engineering B107 (2004) 124–133

ENGINEERING B

www.elsevier.com/locate/mseb

Porosity and density of spark-processed silicon☆

J.G. Polihronov, T. Dubroca, M. Manuel, R.E. Hummel*

Department of Materials Science and Engineering, University of Florida, 216 Rhines Hall, P.O. Box 116400, Gainesville, FL 32611, USA

Received 8 April 2003; received in revised form 17 October 2003

Abstract

Spark-processed Si (sp-Si) is a porous solid-state material. Due to the nature of its structure and morphology, the traditional methods for porosity measurements cannot be utilized. Using the measure theory and the expected value theorems of stereology, we have calculated the porosity of sp-Si to be 43%. Stereological analysis was applied to sp-Si specimen, prepared within a fixed set of growth parameters. Over 60 cross-sectional scanning electron micrographs of the specimen were utilized in this work. The sp-Si sample has a characteristic cylindrical symmetry due to the uniform surface resistance of the Si substrate and to the random nature of spark processing. However, sp-Si is not isotropic, uniform and random (IUR), exhibiting radial and axial anisotropy of porosity. To avoid bias in the calculation, we chose random areas of the cross-sectional surface of sp-Si and calculated their porosities. The calculated values entered into a weighted statistical distribution, in which the statistical weights were determined from the symmetry properties of the sample. The statistical approach and the fact that volume is an additive quantity, allowed us to use a two-dimensional population of points in the calculation of the three-dimensional pore volume fraction and to satisfy the requirement for IUR sample.

In the course of the present work we examined fourteen sp-Si samples, prepared under different processing conditions. Ten of these samples were studied qualitatively by measuring the area of the pores relative to the total area in a cross-sectional cut of the sample. Four samples were studied quantitatively using the stereological method outlined above and exhibited porosities in the neighborhood of 43%. One of these studies is described in detail in the present paper and provides a consistent value for the porosity of sp-Si materials, processed in air.

Small-spot X-ray photoelectron spectroscopy studies of sp-Si were used in the calculation of its density. In the case of inhomogeneous materials, the density is a weighted (with respect to volume) average of the densities of all participating phases. Taking into account the already calculated porosity, we have estimated the density of sp-Si to be 1.36 g/cm^3. The main contribution to this value comes from amorphous SiO_2, which occupies most of the volume of sp-Si.
© 2003 Elsevier B.V. All rights reserved.

Materials studied: Spark-processed silicon; Silica; Porous media; Phosphors

Keywords: Stereology; Porosity; Spark-processed silicon; Inhomogeneous materials; Density

1. Introduction

There are a variety of Si-based materials, which offer a variety of physical properties ranging from insulating to highly conductive. A subclass of these materials has light-emitting properties and has been an object of increasing interest in the past decade. However, the physical nature of the light-emitting Si-based materials has presented some challenges in the attempts to study their local atomic structure and other physical properties closely related to it. The reason for that is the inhomogeneous structure of such materials. Light-emitting Si achieved by laser ablation [1], porous Si [2] and a variety of porous silica [3–8] have light-emitting properties and are inhomogeneous in most cases. The bulk of these materials usually contains mixtures of phases—crystalline, amorphous, surface oxide layers and the frequently present voids (pores).

Technological application of the above materials requires deposition of metal contacts or other thin films on their surface. In such procedures, surface and volume porosity of the underlying material is quite important, since it can allow or disallow smooth and continuous surface coverage. Thus, structural characterization and understanding of morphology

☆ Based on a dissertation submitted by J. Polihronov as a partial fulfillment of the requirements for the degree of Doctor of Philosophy at the University of Florida.

* Corresponding author. Tel.: +1-352-392-6667; fax: +1-352-392-6359.

E-mail address: rhumm@mse.ufl.edu (R.E. Hummel).

0921-5107/$ – see front matter © 2003 Elsevier B.V. All rights reserved.
doi:10.1016/j.mseb.2003.10.112

are vital if one is to develop a successful contact deposition process.

The present work represents a study of light-emitting, spark-processed Si (sp-Si) and its topological and structural properties. sp-Si has stable photoluminescence (PL) [9], which is highly resistant against aging, UV irradiation and thermal annealing up to 1100 °C [10]. In addition, sp-Si based electroluminescent devices have successfully been built [11–13] and are currently undergoing a process of optimization. Electroluminescent sp-Si devices are usually prepared in air, utilizing short spark processing times (10–20 s). The material used in the present work was prepared under identical conditions.

The bulk of sp-Si is highly inhomogeneous and porous. Its morphology and structure have not been studied so far. Understanding of these properties has value from a physical point of view; it can be also used to provide further insights for improved metal contact deposition techniques.

2. Method

The study of sp-Si porosity presents a serious challenge. The traditional methods for porosity measurements cannot be applied due to the nature of sp-Si growth and morphology. Surface atom adsorption techniques are not applicable, since sp-Si contains a large portion of internally embedded, closed pores (Fig. 1). The techniques that involve pore filling are excluded for the same reason. In addition, the bulk contains pores with dimensions in the order of nanometers. Filling of such pores with liquid may not be complete and would introduce an unpredictable error in the measurement. Calculation of the porosity through mass measurements is possible, however this method requires also precise volume measurements. There were a number of attempts to utilize this technique, but these efforts did not yield useful results. The main obstacle was the porous surface of sp-Si, which contains features varying in dimensions from the micrometer scale to the nanoscale. The volume could not be measured with sufficient precision since the upper surface could not be mapped correctly. Additional difficulties arise from the fact that the sp-Si material is not simply deposited on a Si substrate but extends into it, thereby occupying a certain volume in the substrate, which is not easy to estimate. In other words, the underlying surface between the sp-Si and the Si substrate cannot be mapped correctly either.

Solution to these problems was achieved by the application of stereological measurements. The expected value theorems of stereology allow the calculation of volume fraction of phases, surface area per unit volume, average feature size and feature perimeter, to name a few. Detailed description of the various stereological techniques can be found in Ref. [14] and the references therein.

In the measure theory, the volume $V\Omega$ of a set of points Ω (in three-dimensional space) is defined as a measure of the set Ω. The measure of Ω can also be expressed as a function f, which associates a number $V\Omega$ with the set Ω:

$$V_{\Omega} = f(\Omega) \tag{1}$$

Using the Peano–Jordan measure in three-dimensional space, we can state that the volume $V\Omega$ of the set Ω is proportional to the number of points in Ω, and the functional dependence f (Eq. (1)) has an integral form:

$$V_{\Omega} \propto \int_{\Omega} \mathrm{d}p = \int_{\Omega} \mathrm{d}x\,\mathrm{d}y\,\mathrm{d}z, \tag{2}$$

where dp is the density of points in three-dimensional space, $\mathrm{d}p = \mathrm{d}x\,\mathrm{d}y\,\mathrm{d}z$. The Measure Theory will then allow the

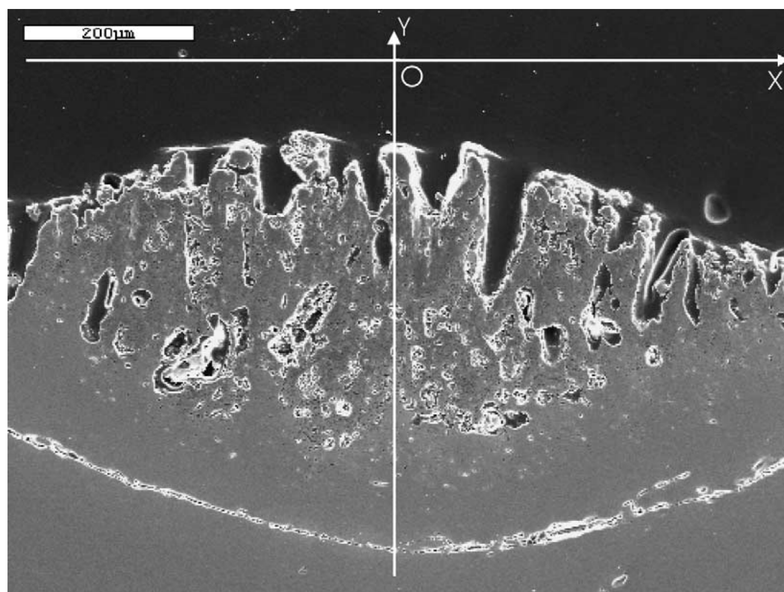

Fig. 1. Cross-sectional SEM micrograph of sp-Si at a magnification of 120×. Y is the axis of symmetry, X is a radial axis.

calculation of the ratio of two volumes of three-dimensional sets Ω_1 and Ω_2 as a ratio of their corresponding measures:

$$\frac{V_{\Omega_1}}{V_{\Omega_2}} = \frac{f(\Omega_1)}{f(\Omega_2)}. \quad (3)$$

Applied to the case of sp-Si, this ratio will be

$$\langle P_\mathrm{p}\rangle^{\mathrm{porosity}} = \frac{V(\mathrm{voids})}{V(\mathrm{entire\ sample})} = \frac{f(\mathrm{voids})}{f(\mathrm{entire\ sample})} = \frac{\int_{\mathrm{voids}} \mathrm{d}p}{\int_{\mathrm{entire\ sample}} \mathrm{d}p} = \frac{\int_{\mathrm{voids}} \mathrm{d}x\,\mathrm{d}y\,\mathrm{d}z}{\int_{\mathrm{entire\ sample}} \mathrm{d}x\,\mathrm{d}y\,\mathrm{d}z} = V_\mathrm{p}, \quad (4)$$

where V_p is the volume fraction of porosity. The above equation can be applied directly for calculation of porosity of sp-Si and its form will be:

$$\langle P_\mathrm{p}\rangle^{\mathrm{porosity}} = \frac{\text{measure of the set of points in the porous phase}}{\text{measure of the set of points in the entire sample}} = V_\mathrm{p} \quad (5)$$

where P_p is the so-called “point fraction”. This equation allows us to study the properties of a population of points in two-dimensional space and apply the result to the three-dimensional structure of the sample.

It is very important to note, that the expression (5) is valid only for samples, which are IUR, i.e. *isotropic uniform random*. The application of (5) to a sample, which is not IUR will lead to a biased result.

sp-Si presents a challenge, since the sp-Si sample is not IUR, but exhibits anisotropy of porosity along the X (radial anisotropy) and Y axes (axial anisotropy, Fig. 1). To avoid bias, we need to calculate an average porosity of the sample, which removes the anisotropy effect. Therefore, we have proceeded as follows:

(1) A sample of sp-Si was cut in a cross-sectional manner (Fig. 1).
(2) The sample was embedded in a resin and fine-polished with diamond powder to produce a smooth cross-sectional surface.
(3) The image of the cross-sectional surface was captured using scanning electron microscope (SEM) at a magnification of 120× (Fig. 1).
(4) A line grid was placed over the image. The spark-processed area (defined by the surface and the interface lines in Fig. 1) was divided into 154 numbered tiles. Each tile is a square having a side of 44.4 μm.
(5) The set of 154 tiles was subdivided into 32 groups of consecutive tiles. Each group contains four or five tiles.
(6) From each group, we selected randomly one tile as follows:

    tile number 4;
    tile number (4 + 5);
    tile number (9 + 4);
    tile number (13 + 5), etc.

    This process of random selection provided us with 32 tiles with numbers 4, 9, 13, 18, 23, ...
(7) SEM micrographs at magnifications 650× were taken for each of the 32 random tiles. At this magnification, nanopores could not be studied.
(8) Linear grids were placed over the images of each tile and the porosity was calculated from Eq. (5). The numerator is the number of grid intersections over voids (marked with bright circles, Fig. 2), while the denominator in (5) is the total number of grid intersections.

Since sp-Si also contains pores with nanometer-scale dimensions, they have to be taken into consideration when porosity is calculated. Since a magnification of 650× is insufficient for counting of nanopores, we prepared a second set of SEM micrographs of the above 32 tiles, captured at a magnification of 3000× and applied Eq. (5) to calculate the nanoporosity (Fig. 3). The magnifications of 3000× showed sufficient detail and were not improved with increase of magnification. To avoid duplicate pore counting, all high-resolution micrographs were captured from random areas (within the given tile) that do not contain macropores.

Thus, the total porosity P_i^{total} measured on a tile i, is determined to be

$$P_i^{\mathrm{total}} = P_i^{\mathrm{micro}} + P_i^{\mathrm{nano}}. \quad (6)$$

One also needs to take into account the fact, that the sp-Si sample has cylindrical symmetry (Fig. 1) with an axis of symmetry Y. The cylindrical symmetry is contingent upon the characteristics of spark processing. Normally, the Si substrate is uniformly doped and therefore its resistivity is the same throughout its bulk. Once a spark event occurs at a given point of the substrate surface, the resistivity of this particular locality increases, since spark processing creates clusters of highly resistive surface compounds [10]. The next spark event will most probably occur at another surface point with lower resistivity. Each spark occurs at a surface spot such, that the resistance between the sparking tip and the spot is minimal. This fact guarantees the circular surface pattern, observed after spark processing of Si.

Since each tile is positioned at some distance from the Y-axis (Fig. 1), it represents a volume ΔV_i

$$\Delta V_i = 2\pi h R_i\,\Delta R, \quad (7)$$

where R_i is the distance between the Y-axis and the geometrical center of the tile i and $h = \Delta R$ is the tile side. Then, to each tile we associate a statistical weight w_i

$$w_i = \frac{\Delta V_i}{\sum_{k=1,\ \mathrm{all\ 32\ tiles}}^{32} \Delta V_k}. \quad (8)$$

The total porosity of the sp-Si sample will be

$$P_{\mathrm{sp\text{-}Si}} = \sum_{i=1,\ \mathrm{all\ 32\ tiles}}^{32} (P_i^{\mathrm{micro}} + P_i^{\mathrm{nano}})\,w_i, \quad (9)$$

which takes into account the fact that the volume is an additive quantity.

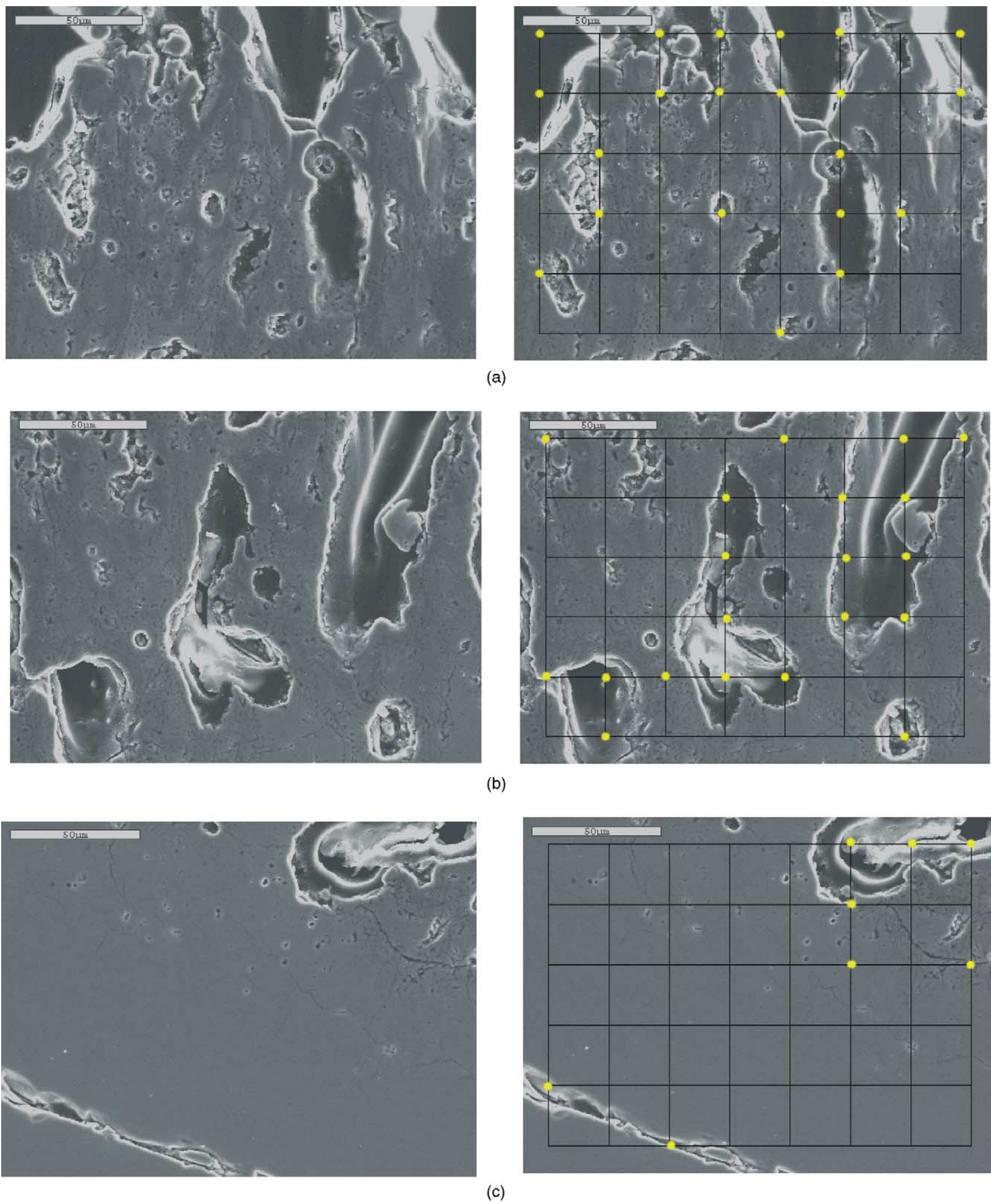

Fig. 2. Selected tile images of the sp-Si sample at a magnification of 650×. The right column displays rectangular grids positioned over the images of the material. The bright circular marks denote that the grid intersection resides over a void. (a) Near-surface image; (b) image of the sp-Si bulk; and (c) near the interface sp-Si/Si.

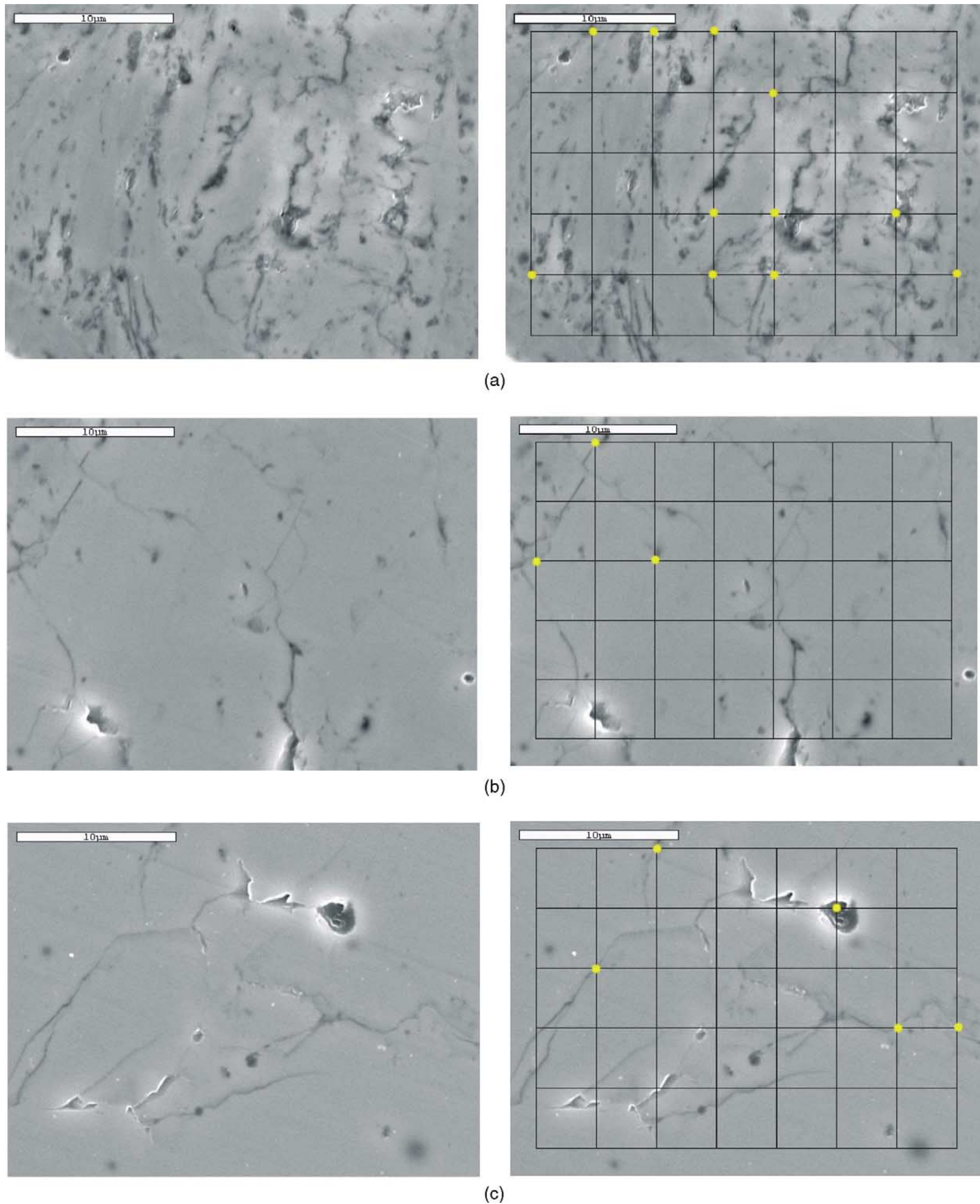

Fig. 3. Selected tile images of the sp-Si sample at a magnification of 3000×. The right column displays rectangular grids positioned over the images of the material. The bright circular marks denote that the grid intersection resides over a void. (a) Near-surface image; (b) image of the sp-Si bulk; and (c) near the interface sp-Si/Si.

3. Results and discussion

The point count measurement contains a certain error. It is due mainly to microscopy edge effects near the pore boundaries, which appear bright (Fig. 2).

In all cases when a grid intersection was positioned over a bright pore-edge area, we proceeded as follows:

(i) the corresponding mark was counted into the porosity if the intersection was positioned within the inner (towards the pore) lying half of the bright area;

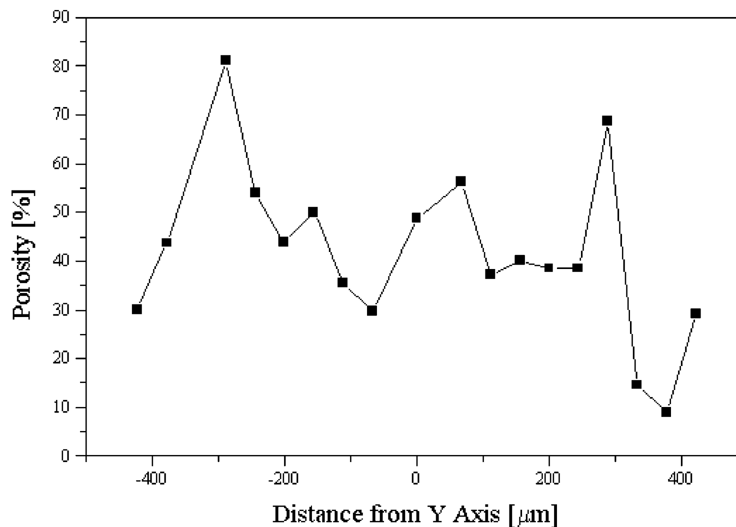

Fig. 4. Radial distribution of porosity in sp-Si. The lines are a guide to the eye. Each data point is calculated with an average accuracy of 4%.

(ii) the corresponding mark was counted into the porosity and also counted as error if the intersection was positioned within the outer lying half of the bright area.

Thus, the calculated total porosity is an upper limit to the true porosity, and the error corresponds to an interval of possible lower values.

The linear grids used in the stereological measurements consist of lines with finite thickness. The points of intersection of two lines were therefore considered to be located on the pixel at the upper right corner of the intersection.

The edge effects and the error associated with them were largely absent in the high-resolution images for nano-porosity calculation. Still, some error was generated in these cases due to the fact, that certain localized areas were not flat. The marks within them were counted into the error of the measurement and into the nano-porosity as well. As a result, the error of the nano-porosity count is larger compared to its counterpart in the macro-porosity measurement.

Applying the Eq. (9), we calculated the micro-porosity of sp-Si to be 26.0% with an accuracy of 2.0%. The nano-porosity is 16.9% with an accuracy of 4.0%. Therefore, the total porosity of sp-Si is calculated to be 42.9% with an accuracy of 6.0%. This should be interpreted to mean that true porosity lies within an interval with numerical length of 6%, defined by the upper limit of 42.9% and the lower limit of 36.9%:

$$36.9\% \leq P_{\text{sp-Si}} \leq 42.9\%. \qquad (10)$$

Figs. 4–7 show distributions of porosity in different directions, measured by averaging over layers of the probe. While the error of the individual points of the distributions

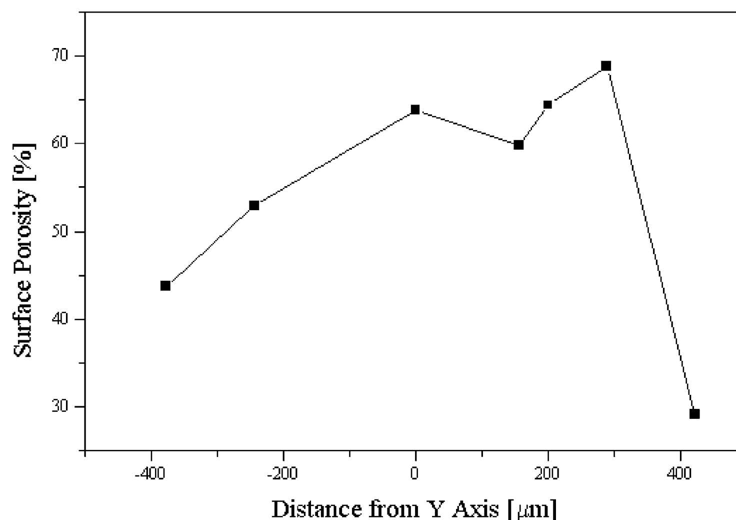

Fig. 5. Radial distribution of porosity in a layer with thickness of 100 μm at the surface of sp-Si. The lines are a guide to the eye. Each data point is calculated with an average accuracy of 4%.

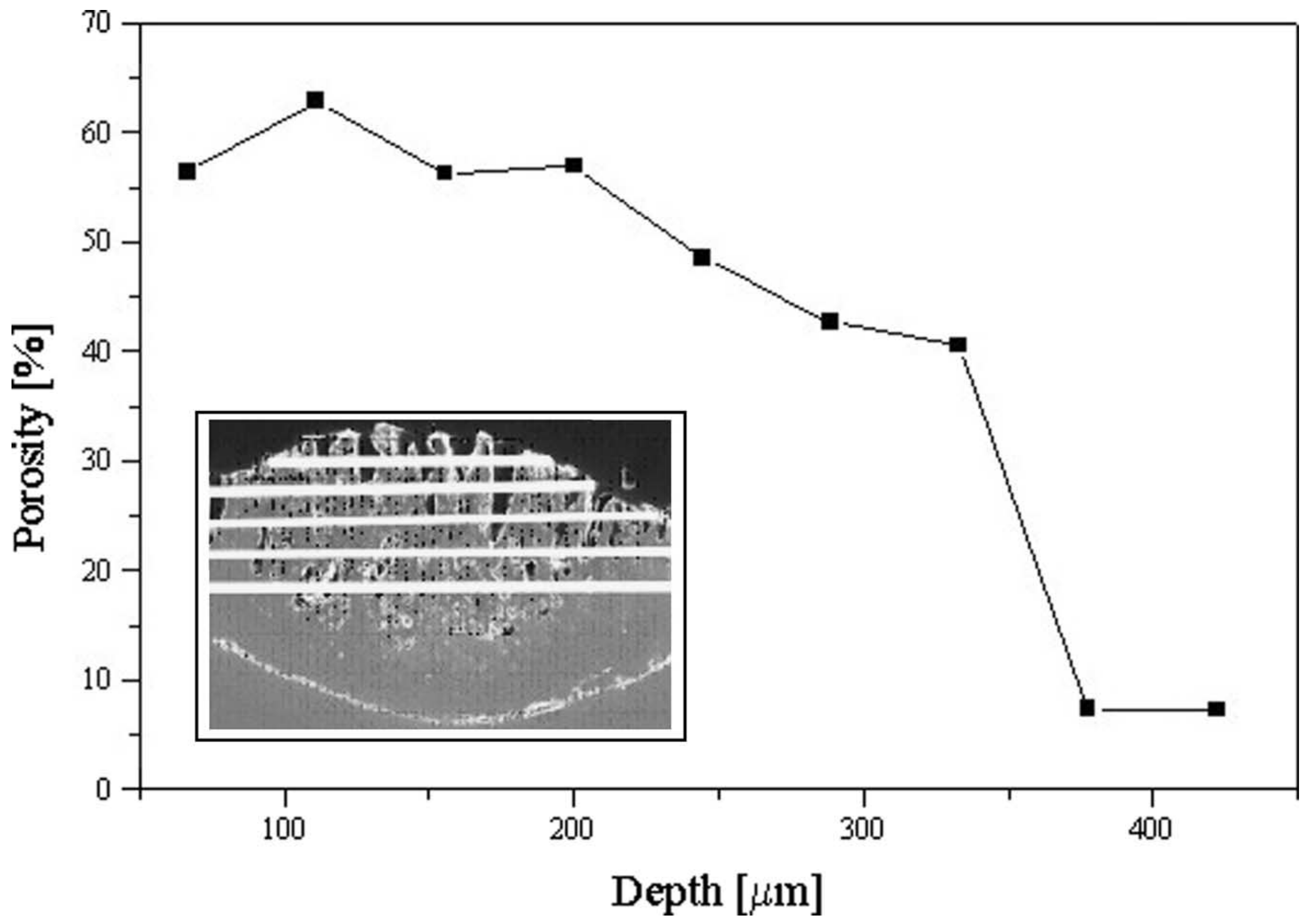

Fig. 6. Depth profile of porosity in sp-Si. The averaging with depth has been performed over horizontal slabs, as shown in inset. Each data point is calculated with an average accuracy of 4%.

may vary between 0 and 8.3%, the average error of each point is estimated to be 4%.

Fig. 4 depicts the radial distribution of porosity. The term "radial" refers to the cylindrical symmetry of the sp-Si sample, where Y is the axis of the cylinder, and one of its radii lies along the X-axis (Fig. 1). The porosity is lowest at the sample edges and exhibits peaks symmetrically positioned with respect to the Y-axis. It can also be noticed that the porosity can occupy values higher than 80% in certain small localities. Another distribution is shown on Fig. 5. This is the radial porosity distribution of a surface layer with thickness of approximately 100 μm. P occupies high values even at the edges and is peaked in the middle of the sample. Under such circumstances, metal contact deposition on the sp-Si surface will create a better coverage in the periphery of the sample and will be largely discontinued in its center.

Fig. 6 displays a depth profile of porosity, achieved by averaging over horizontal slabs with thickness of around 50 μm. Fig. 7 depicts a porosity depth profile, which has been achieved by averaging over layers with the same thickness as above. In this case, all points of the layers are equally distant from the surface. Both profiles show non-linear decrease of porosity, having lowest value of around a few percent near the sp-Si/Si interface.

4. Density of sp-Si

The estimate of the density of sp-Si is based on a small-spot X-ray electron spectroscopy (XPS) depth profile of the material, published in [10] (Fig. 8). Since sp-Si is inhomogeneous, its average density will be

$$\rho_{\text{sp-Si}}^{\text{solid phase}} = \frac{m_{\text{sp-Si}}}{V_{\text{sp-Si}}} = \sum_k \rho_k \left(\frac{V_k}{V_{\text{sp-Si}}} \right), \quad (11)$$

where the sum is taken over all volumes of the various phases in sp-Si. The factor in the brackets represents the statistical weight of the density ρ_k of the corresponding phase k. It should be noted that (11) is calculated entirely based on information from the XPS measurement and as such it represents the density of the solid phase only. Then, the true density of sp-Si will be

$$\rho_{\text{sp-Si}} = \rho_{\text{sp-Si}}^{\text{solid phase}} (1 - P_{\text{sp-Si}}), \quad (12)$$

Fig. 7. Depth profile of porosity in sp-Si. The averaging with depth has been performed over layers, equidistant from sp-Si surface (inset). Each data point is calculated with an average accuracy of 4%.

where $P_{\text{sp-Si}}$ is the porosity of the material, calculated in Eq. (9).

To estimate (12), certain approximations are adopted. Based on previously published data for plasma-grown Si

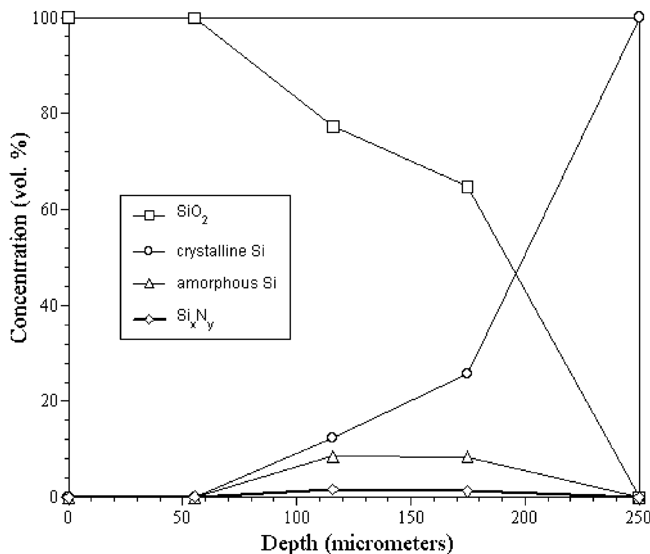

Fig. 8. Small-spot XPS data for sp-Si (adapted from [10]).

oxynitride materials with similar depth profiles of SiO_2, Si and Si_3N_4 [15–23], we assume the connecting lines in the XPS diagram of sp-Si (Fig. 8) to represent data points.

In detail, this assumption is based on the following:

(i) In the above references, the depth profile of N is typically peaked near the oxide/Si interface for all as-grown samples, which have not been subjected to additional treatment.
(ii) The quoted references show the concentration of SiO_2 to decrease in a non-linear fashion, similarly to the profile shown in Fig. 8, and the concentration of Si increases in a similar pattern.

Unless the plasma-grown Si oxynitride films have been subjected to a secondary treatment (annealing in N, implantation, secondary plasma treatments), the depth profiles of SiO_2, N and Si exhibit behavior similar to the approximation shown on Fig. 8.

This approximation allows us to generate data points for the concentration of SiO_2, crystalline Si (c-Si), amorphous Si (a-Si) and Si_xN_y for 250 horizontal slabs of sp-Si having thickness of 1 μm each (as in Fig. 6, inset). As a second approximation, we assume for Si_xN_y $x = 3$, $y = 4$. This allows us to use the density of Si_3N_4 in the calculation.

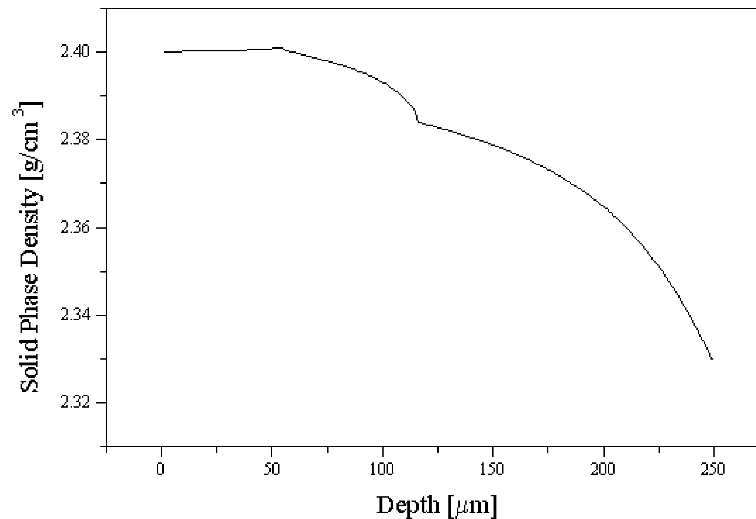

Fig. 9. Depth profile of sp-Si density. The averaging with depth has been performed over 250 horizontal slabs, as shown in the inset of Fig. 6.

The densities of the participating chemical compounds are: ρ(a-SiO_2) = 2.4 g/cm^3 [24], ρ(c-Si) = 2.3 g/cm^3 [25], ρ(a-Si) = 2.2 g/cm^3 [26,27] and ρ(a-Si_3N_4) = 3.0 g/cm^3 [28]. Using these densities and Eq. (11), we determine the average solid phase density of sp-Si in each of the 250 slabs. The results are presented in Fig. 9. The points of discontinuity are due to the first approximation in the calculation. ρ decreases from the value of 2.4 g/cm^3, corresponding to the density of SiO_2, to the value of 2.3 g/cm^3, corresponding to the density of c-Si.

The average density for the entire solid phase is determined by Eq. (11), where the averaging is conducted over the 250 slabs. However, since the surface of sp-Si and the interface sp-Si/Si substrate cannot be mapped correctly, the precise volume of each slab cannot be estimated. In order to avoid this obstacle, we assumed all slabs to have equal volumes. Mathematically, this means that their densities enter the sum (11) with equal weights and artificially increase the volume contributions from the surface and interface areas, which are otherwise small. Therefore, the calculated value of the sp-Si density is an estimate, which overstates the participating amounts of a-SiO_2 and c-Si.

Our calculation determines $\rho_{\text{sp-Si}}^{\text{solid phase}}$ to be 2.38 g/cm^3. Since most of the volume of the material is occupied by SiO_2 (ρ(a-SiO_2) = 2.4 g/cm^3), the value of 2.38 g/cm^3 shows that Si dioxide is the main contributor to the density of sp-Si. The true density of sp-Si, after taking into account the contributions from both the solid phase and the voids in the material, is calculated by Eq. (12):

$$\rho_{\text{sp-Si}} = 1.36\ \text{g/cm}^3.$$

5. Conclusions

The total volume fraction of porosity in sp-Si is calculated to be approximately 43%. The surface porosity of the material is high, reaching up to 69% in the central area of the sample. This study was conducted for sp-Si specimen, grown within a fixed set of processing parameters. Despite that the variation of the growth parameters may influence the microstructure of the material, our results have general applicability and describe a non-traditional method for successful porosity measurements. The density of sp-Si is estimated to be 1.36 g/cm^3. The main contribution to the density of this material comes from a-SiO_2, which occupies most of its volume.

Acknowledgements

We are grateful to Prof. R. DeHoff for the useful discussions on IUR samples in stereology and for his suggestions and encouragement. This work was financially supported through a grant from the National Science Foundation (DMR).

References

[1] R.E. Hummel, M.E. Stora, N. Shepherd, S. Yu, F. Fajardo, J. Porous Mater. 7 (2000) 131.
[2] L.T. Canham, Appl. Phys. Lett. 57 (1990) 1046.
[3] H. Wong, Microel. Reliab. 42 (2002) 317.
[4] A.M. Danilevskii, V.B. Shuman, A.Yu. Rogachev, P.A. Ivanov, Semiconductors 29 (1995) 1063.
[5] A. Konstantinov, C.I. Harris, A. Henry, B. Monemar, E. Janzen, in: 22nd International Conference on the Physics of Semiconductors, vol. 3, 1995, p. 2157.
[6] V. Petrova-Koch, T. Muschik, Thin Solid Films 255 (1995) 246.
[7] V. Petrova-Koch, T. Muschik, A. Kux, B.K. Meyer, F. Koch, V. Lehmann, Appl. Phys. Lett. 61 (1992) 943.
[8] Ya.O. Roizin, A. Alexeev-Popov, S.A. Gevelyuk, D.P. Savin, E. Mugenski, I. Sokolska, E. Rysiakiewicz-Pasek, K. Marczuk, Phys. Chem. Glasses 37 (1996) 196.
[9] R.E. Hummel, S.-S. Chang, Appl. Phys. Lett. 61 (1992) 1965.

[10] R.E. Hummel, Photonic and Magnetic Properties of Spark-Processed Silicon in: Silicon-Based Materials and Devices, Vol. I, Chapter 6, Academic Press, 2001, pp. 237–265.
[11] N. Shepherd, R.E. Hummel, Phys. Status Solidi 197 (2003) 222.
[12] N. Shepherd, R.E. Hummel, J. Phys. Chem. Solids 64 (2003) 967.
[13] J. Yuan, D. Haneman, Appl. Phys. Lett. 67 (1995) 3328.
[14] J.C. Russ, R.T. Dehoff, Practical Stereology, second ed., Kluwer Academic Publishers/Plenum Press, New York, 2000.
[15] E.P. Gusev, H.-C. Lu, E.L. Garfunkel, T. Gustafsson, M.L. Green, IBM J. Res. Dev. 43 (1999) 3.
[16] T. Hori, H. Iwasaki, K. Tsuji, IEEE Trans. El. Dev. 36 (1989) 340.
[17] A. Glachant, Thin Solid Films 254 (1995) 54.
[18] K. Nakajima, K. Kimura, A. Kurokawa, S. Ichimura, H. Fukuda, Jpn. J. Appl. Phys. 40 (Pt. 1) (2001) 4011.
[19] Y. Saito, Appl. Phys. Lett. 68 (1996) 800.
[20] M.L. Monagan, T. Nigam, M. Houssa, S. De Gendt, H.P. Urbach, P.K. De Bokx, Thin Solid Films 359 (2000) 197.
[21] B. Brijs, J. Deleu, T. Conard, H. De Witte, W. Vandervorst, K. Nakajima, K. Kimura, I. Genchev, A. Bergmaier, L. Goergens, P. Neumaier, G. Dollinger, M. Dobeli, Nucl. Instr. Meth. Phys. Res. B 161–163 (2000) 429.
[22] R.P. Vasquez, A. Madhukar, F.J. Grunthaner, M.L. Naiman, J. Appl. Phys. 59 (1986) 972.
[23] M. Ueda, A.F. Beloto, H. Reuther, S. Parascandola, Surf. Coat. Technol. 136 (2001) 244.
[24] N. Awaji, S. Ohkubo, T. Nakanishi, Y. Sugita, K. Takasaki, S. Komiya, Jpn. J. Appl. Phys. 35 (Pt. 2) (1996) L67.
[25] N.I. Koshkin, M.G. Shirkevich, Handbook of Elementary Physics, Mir Publishers, Moscow, 1977.
[26] A.F. Ruppert, P.D. Persans, G.J. Hughes, K.S. Liang, B. Abeles, W. Landford, Phys. Rev. B 44 (1991) 11381.
[27] J.S. Custer, M.O. Thompson, D.C. Jacobson, J.M. Poate, S. Roorda, W.C. Sinke, F. Spaepen, Appl. Phys. Lett. 64 (1994) 437.
[28] T. Hirai, T. Goto, J. Mater. Sci. 16 (1981) 2877.